Environmental Pollution 390 (2026) 127453

Contents lists available at ScienceDirect

Environmental Pollution

journal homepage: www.elsevier.com/locate/envpol

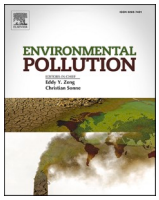

Analysis of microplastics and nanoplastics emerged from polyethylene bags and polyethylene terephthalate bottles by an artificial intelligence-enabled tool☆

Hadi Rezvani [a], Mihir Kapadia [a], Julia Costantino [a], Navid Zarrabi [b], Sajad Saeedi [b,c], Nariman Yousefi [a,*]

[a] Department of Chemical Engineering, Toronto Metropolitan University, 350 Victoria Street, Toronto, Ontario, M5B 2K3, Canada
[b] Department of Mechanical, Industrial, and Mechatronics Engineering, Toronto Metropolitan University, 350 Victoria Street, Toronto, Ontario, M5B 2K3, Canada
[c] Department of Computer Science, University College London, London, United Kingdom

ARTICLE INFO

Keywords:
Microplastics
Nanoplastics
Polyethylene (PE)
Polyethylene Terephthalate (PET)
Artificial intelligence

ABSTRACT

This study presents a comprehensive and comparative analysis of the emergence of micro- and nanoplastics (MNPs) from polyethylene (PE) plastic bags and polyethylene terephthalate (PET) water bottles. We subjected these polymers to simulated mechanical and photodegradation conditions in an isolated chamber for 12 weeks to understand their environmental implications and degradation mechanisms. We analyzed 614 and 3924 plastic particles that emerged from PE and PET, respectively, using an artificial intelligence (AI) enhanced automatic annotation tool (FastSAM) focusing on MNPs' particle count, size distribution, and morphology. This innovative approach combines comprehensive simulation of environmental conditions with AI-enabled image analysis, providing detailed insight into the relative contributions of PE and PET products to plastic pollution. Our findings indicate that PET fragments more readily into smaller particles, with a higher proportion of nanoplastics (57.6 %) than PE (24.9 %). The concentration of the emerged particles was found to be 4.17 million particles/L (0.07 ppm) for PE and 27.8 million particles/L (0.18 ppm) for PET. Characterization techniques, including dynamic light scattering (DLS), scanning electron microscopy (SEM), Fourier-transform infrared spectroscopy (FTIR), and X-ray photoelectron spectroscopy (XPS) were used to examine both bulk plastics and the MNPs that emerged from them.

1. Introduction

Plastic pollution is a critical environmental issue with far-reaching impacts on ecosystems and human health. The pervasive presence of micro- and nanoplastics (MNPs) in the environment has become a significant concern, necessitating a deeper understanding of their sources, degradation mechanisms, and environmental consequences. Current statistics show that in 2015, 55 % of plastic waste was discarded, and 25 % incinerated (Kibria et al., 2023). Most discarded plastics gradually fragment into MNPs under sunlight and mechanical forces (Novakovic et al., 2023), highlighting the urgent need for a deeper understanding of plastic degradation mechanisms and their environmental consequences. MNPs are found globally in soil, water, and air (Dube and Okuthe, 2023; Isobe and Iwasaki, 2022; Mason et al., 2018). Animals ingest MNPs, which travel up the food chain and eventually reach humans through seafood and water (Yong et al., 2020). MNPs also serve as sources and carriers of pollutants, helping toxic chemicals leach into the environment (Xu et al., 2024). Furthermore, their small size and large surface area make them effective adsorbents for various contaminants (Brewer et al., 2021).

Despite significant advances in the detection and characterization of MNPs using techniques like dynamic light scattering (DLS), scanning electron microscopy (SEM), and Fourier-transform infrared spectroscopy (FTIR), there is a lack of comprehensive data on the emergence of MNPs from commercial plastic products under controlled environmental conditions[4]. Previous studies have identified various sources of MNPs, such as plastic bottles (Mintenig et al., 2018; Schymanski et al., 2018), polypropylene (PP) caps (Giese et al., 2021; Winkler et al., 2019), car

☆ This paper has been recommended for acceptance by YING GUO.

* Corresponding author.
E-mail address: nariman.yousefi@torontomu.ca (N. Yousefi).

https://doi.org/10.1016/j.envpol.2025.127453
Received 5 September 2025; Received in revised form 7 November 2025; Accepted 27 November 2025
Available online 28 November 2025

tires (Knight et al., 2020), washing machines (Cai et al., 2020; Kelly et al., 2019), and even tea bags (Hernandez et al., 2019), stressing their widespread environmental impact.

The increase in the generation and environmental transport of MNPs necessitates advancing our understanding of their emergence from bulk plastics. Crucial gaps persist in understanding the complex weathering processes of bulk plastics and the consequential release of MNPs. Moreover, while previous studies have primarily focused either on environmental microplastics (MPs) or the degradation of neat polymers, limited attention has been given to the aging process of real, processed-affected consumer polymers and the emergence of MNPs from them. Additionally, the need for a more streamlined and automated approach to detect, identify, and quantify MNPs in aquatic environments is increasingly pressing. Recently, applying microscopy techniques with artificial intelligence (AI) enhanced image analysis and machine learning (ML) techniques have been proposed as a promising avenue, albeit with gaps in nanoplastic (NP) analysis and a need for more data on MNPs released from consumer plastics (Chen et al., 2024; Liu et al., 2023). Understanding the degradation behaviour of consumer-grade, processed polyethylene (PE), such as those used in plastic shopping bags, and polyethylene terephthalate (PET), which is primarily used in single-use plastic water bottles, is crucial as these polymers constitute a large number of the single-use plastic waste and dominate aquatic plastic pollution (Ibor et al., 2023).

In this study, we aim to bridge critical gaps in understanding the degradation and environmental implications of widely used consumer plastics by utilizing a novel combination of advanced characterization techniques, AI-enhanced data analysis, and comparative methodologies. Unlike previous studies that often focus on individual plastic types or simplified conditions, our work directly compares the degradation behaviours of consumer plastics that have undergone processing, such as PE plastic bags and polyethylene PET water bottles, under simulated environmental conditions. The simulated environment includes UV exposure and mechanical stress in a controlled degradation chamber that enables continuous monitoring of MNP emergence. At the same time, the integration of ML for particle identification represents a significant advancement in the rapid and accurate quantification of MNPs. By correlating physical and chemical transformations in these polymers to their environmental fate, we provide detailed insights into the mechanisms driving MNP release.

2. Materials and methods

2.1. Polymer degradation and MNP emergence

A single commercial brand of PE shopping bags and one brand of PET water bottles were collected from local shops in Toronto to represent typical consumer-grade plastics. This approach minimized variability in additive composition and manufacturing while maintaining environmental relevance. We placed six pieces of PE and PET (2×2 cm^2) in separate 500 ml glass photoreactors filled with 300 ml deionized (DI) water to serve as sources for MNP emergence in the degradation chamber depicted in Fig. S1. DI water used in all experiments was Type II reagent-grade (Fisher Scientific, Cat# 23751628) with resistivity >10 MΩ/cm, silicates <0.05 mg/L and pH 5.5–7.5 at 25 °C. All degradation experiments were performed in an enclosed and isolated setup at Toronto Metropolitan University. The degradation chambers were placed under a chemical fume hood to prevent external particle intrusion.

The chamber provided continuous UV irradiation at an intensity of 50 W/m^2 (254 nm peak) and cyclic mechanical stirring at 300 rpm, with the internal temperature maintained at 25 ± 2 °C and relative humidity at 60 ± 5 %. The specific intensity and wavelength of the UV, which is more intense than what is encountered in the environment, was selected to accelerate the degradation of plastics in 12 weeks by intensifying photochemical reactions under controlled laboratory settings. The temperature and humidity closely match the average summer environmental conditions in Toronto, while the mechanical agitation simulates moderate surface-water mixing, collectively approximating accelerated weathering. Our previous work provides details on the in-house-built degradation chamber and protocols for the degradation and characterization of the polymers and MNPs (Rezvani et al., 2025). White quartz sand (Sigma-Aldrich, Cat. No. 274739, 50–70 mesh particle size) was used in some experiments to simulate natural mechanical abrasion during degradation tests. For experiments conducted in dark, the glass beakers were covered by several layers of aluminum foil. The results presented in this study are obtained from three independently-run degradation experiments.

2.2. Characterization methods

The emergence of MNPs was monitored over a 12-week degradation period using DLS (Malvern Zetasizer Nano ZS) to observe particle size changes. The morphology of bulk plastics before and after degradation was analyzed with an SEM (JEOL JSM-6380LV) at 20 kV using secondary electrons. After 12 weeks, MNPs were collected by vacuum filtering 50 ml of the aqueous medium through track-etched polycarbonate membranes (MilliporeSigma™ Isopore™ Membrane Filters, 0.2 μm). These membranes were sputter-coated with gold and analyzed using SEM. An XPS (Thermo Scientific K-Alpha) with an Al-Kα X-Ray source operating at 10^{-8} mbar vacuum was used to study the surface chemistry of the bulk polymers before and after degradation, as well as the emerged MNPs. Survey scans and high-resolution C_{1s} and O_{1s} spectra were recorded and deconvoluted using the Avantage software. Additionally, the surface chemistry of the bulk samples was investigated using ATR-FTIR (Agilent Cary 630) with a scanning range from 650 to 4000 cm^{-1}. The carbonyl index (CI) of the bulk polymers before and after degradation was calculated using the obtained spectra. The CI is defined as the ratio of the area under the carbonyl peak (~1750 cm^{-1}) to that of a reference peak that remains constant as the polymer degrades. For PET, the reference peak was the aromatic ring C=C bond at 1508 cm^{-1}, and for PE, it was the methylene group (–CH_2) at 1460 cm^{-1} (S. Gomes et al., 2024).

2.3. Annotation of the SEM micrographs and morphology analysis

To accurately analyze MNPs, we used an AI-assisted technique for particle annotation and image analysis. We analyzed 26 SEM micrographs each for PET and PE using image analysis. Each annotation included comprehensive information such as a particle mask, bounding box, area, diameter, and category. We manually annotated the particles in the micrographs using V7's AI-powered platform (V7 Labs, London, UK), which provides automated and manual annotation tools for image processing. V7 platform ensures high accuracy and consistency ("V7 Darwin | AI Data Labeling & ML Training Data Platform," 2023). The V7 platform integrates the Segment Anything Model (SAM) for zero-shot segmentation. We used FastSAM, an AI-enhanced tool, to automate the annotation of MNPs in the SEM micrographs. Although FastSAM has not been specifically validated on SEM data, prior studies have demonstrated the capability of SAM-based models for microscopic imaging. SAM has also been used in relevant applications, such as μSAM, a specialized SAM-based framework for biological microscopy that significantly accelerates instance segmentation while maintaining high accuracy (Archit et al., 2025). Similarly, deep learning approaches have been applied to SEM micrographs of shale for intelligent identification of microscopic particles, confirming the feasibility of AI-based segmentation in SEM contexts (Zhang et al., 2025). Building on this foundation, we used FastSAM for pre-annotation to accelerate particle segmentation in SEM micrographs. Using this approach, we automatically segmented 46.36 % of particles in PE images and 45.99 % in PET images. The masks generated by FastSAM were exported to the V7 platform for a thorough manual verification and completion by human experts, as shown in Fig. 1. On average, manual annotation of a single particle required

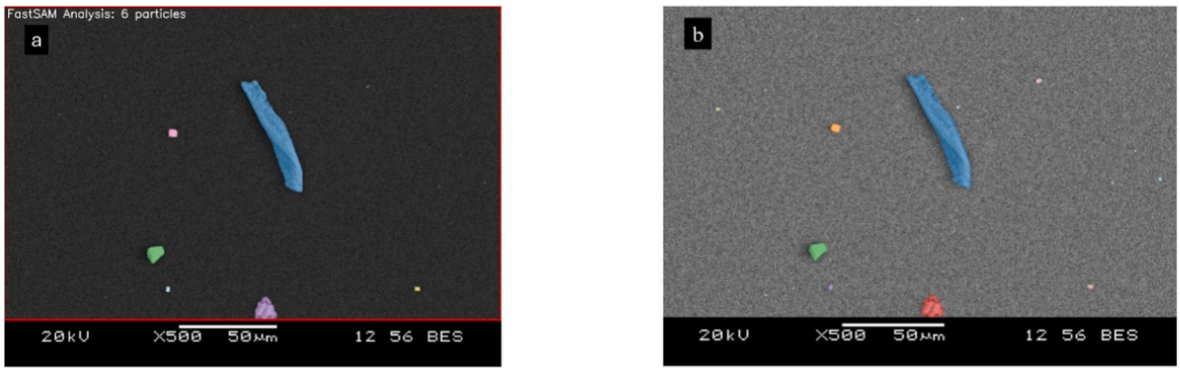

Fig. 1. (a) Pre-annotation generated by FastSAM has successfully detected and annotated 6 PE particles in the micrograph. (b) The human expert verified the FastSAM segmentation and annotated the remaining 4 PE particles.

33.41 s, indicating that FastSAM saved approximately 17.41 person-hours of labeling time.

By leveraging FastSAM's segmentation capabilities, we significantly improve annotation efficiency and precision, reducing the need for extensive manual segmentation. FastSAM's ability to generate multiple segmentation masks for ambiguous prompts is particularly beneficial for MNPs exhibiting irregular shapes and uneven surface charge distributions (Kirillov et al., 2023). This AI-assisted approach enhances the robustness of MNP detection, facilitating more reliable characterization and quantification. We extracted morphological data, including form factor, aspect ratio, roundness, and convexity, and statistically analyzed them to identify significant morphological differences between MNPs emerged from PE and PET. Given that the data was not normally distributed, as confirmed by normality tests (with p-values effectively equal to 0 for all factors), we used non-parametric methods for analysis. Specifically, we conducted Mann-Whitney U tests (Mann and Whitney, 1947) to compare PE and PET across the mentioned factors. The significance level was set at $p < 0.05$. A detailed description of our manual annotation methodology and morphological parameters is provided in our previous study (Rezvani et al., 2024). Statistical analyses and data visualization were performed using OriginPro 2024 (Version 10.1, OriginLab Corporation, Northampton, MA, USA).

3. Results and discussion

3.1. Morphology of the bulk polymers and the emerged MNPs

To monitor MNP emergence, aliquots from the degradation medium (DI water) of each sample were examined using DLS every week. Fig. 2 presents the DLS graphs for PE and PET in weeks 4, 8, 10, and 12. The particle size distribution over 12 weeks shows notable trends. For both PE and PET, the first indication of MNP emergence appeared in the aqueous medium of week 4, close to what has been reported in the literature (Weinstein et al., 2016). The size distribution increased steadily up to week 12. At the same time, the control samples did not show any particles up to week 12, which is proof of no or little contamination in the environmental chamber. After week 12, contamination was observed in the control sample, so we limited the degradation period to 12 weeks. Control samples (DI water only) were analyzed using SEM and energy dispersive spectroscopy (EDS) after the 12-week exposure period. Based on the morphology of the observed particles and their elemental composition, we identified the few detected contaminants as dust particles, consistent with the literature (Malli Mohan et al., 2019); however, these particles were not observed in samples collected during the 12 week period, and were consistently observed after 12 weeks. Representative SEM micrographs and corresponding EDS spectra

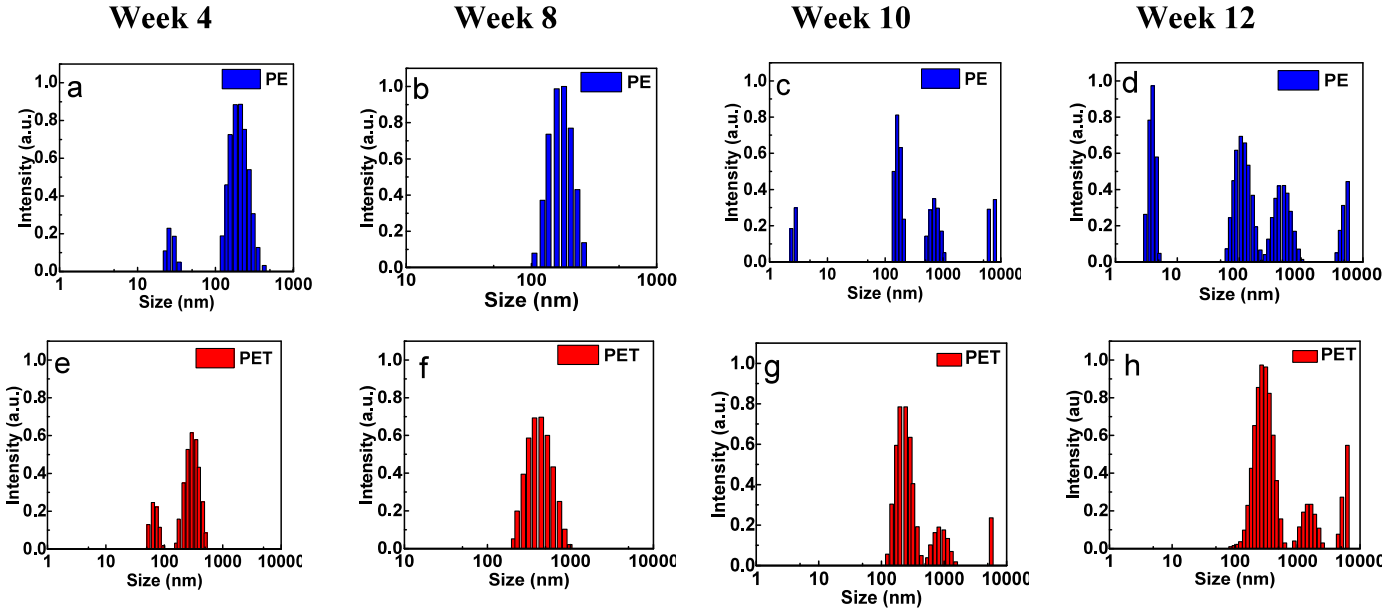

Fig. 2. Distribution of the hydrodynamic diameter of the MNPs emerged from PE plastic bags in (a) week 4, (b) week 8, (c) week 10, (d) week 12, and PET water bottles in (e) week 4, (f) week 8, (g) week 10, and (h) week 12.

of these background particles are provided in the Supporting Information (Fig. S2 and Table S1).

Fig. 2a–d shows the distribution of the hydrodynamic diameter of the emerged MNPs from PE (DLS size distribution) in water for weeks 4–12. The results indicate that nano-sized particles (nanoplastics) remained observable up to week 12, indicating minimal aggregation, likely due to their smaller size or lower particle count, which prevents overshadowing effects from microparticles during DLS experiments.

Based on Fig. 2, the size of PET and PE MNPs increased from a few nanometers to around 10 μm over the 12 weeks span, highlighting the dynamic nature of MNP emergence. This behavior has been observed in PE, PP and polystyrene (PS) (Rezvani et al., 2024). The particles emerged from PET samples (Fig. 2e–h) shifted from a polydisperse size profile in week 4 to a single, broader peak in week 8, suggesting MNP aggregation into larger assemblies. This size increase in PET likely results from surpassing theoretical critical aggregation concentration, promoting cluster formation. The rise in MNP size and distribution broadening indicates an initial phase of nanoplastic emergence from bulk polymers due to photo-oxidation. This is followed by aggregation due to increased surface area and polarity, forming larger particles and eventual MPs. The crack formation process in bulk plastic can also contribute to this pattern (Gao et al., 2024). Crack formation starts when the covalent bonds in macromolecules break due to oxidation, which leads to nanoplastic release from the surface (Kang et al., 2024). Over time, this process contributes to the creation of MPs, as larger pieces break away from the bulk material (Ibrahim, 2024; Li et al., 2021). Research on the size distribution change of the MNPs that emerge from bulk plastic throughout photooxidation is highly valuable, as it gives a clearer insight into the mechanisms involved in generating the particles from bulk. Most of the studies published in this area focus on the emergence of larger MPs due to the limitations of the analysis methods for detecting smaller microparticles and nanoparticles (Julienne et al., 2019; Weinstein et al., 2016).

Typical SEM micrographs of the PE and PET MNPs that emerged after 12 weeks of degradation are presented in Fig. 3, confirming the DLS hydrodynamic size distribution results. Micrographs are taken from the surface of the track-etched PC membranes that were used for filtering aliquots of the degradation medium (DI water). The porous substrate observed is the membrane surface; whereas the particles are the released MNPs. Micrographs of PET MNPs (Fig. 3a and b) show relatively large particles with a broad size distribution, from nanoplastic to MP range, consistent with the DLS findings of increasing MNP size over 12 weeks. Notably, aggregates of small and large particles can be observed, indicating that critical aggregation concentrations have been surpassed, as also shown by the broader peaks in the DLS data. In contrast, PE micrographs (Fig. 3c and d) display fewer MNPs with a narrower size range and less aggregation in line with DLS results, which show PE MNPs maintaining smaller sizes and limited aggregation. These SEM micrographs visually confirm the quantitative DLS data, highlighting differences in the number of emerged MNPs and their agglomeration patterns between PE and PET. While PET MNPs show a wide size range and significant agglomeration, PE MNPs remain smaller and less aggregated.

Microscopic examination of bulk PE and PET surfaces before and after degradation (Fig. S3) reveals significant changes in surface structure due to photooxidation-induced polymer degradation. In PET samples post-degradation (Fig. S3b), flaking and scaling are prominent, suggesting potential sites for the emergence of MNPs. This flaking and scaling can result from chain scission and surface shedding, which are clear signs of polymer degradation and MNP emergence (Maddison et al., 2023). This is in line with the recent studies, which report the formation of small holes, fissures, disintegration, cracks, and grooves after weeks of photooxidation of polymers (Arhant et al., 2019; Dimassi et al., 2023; Ding et al., 2022).

For bulk PE post-degradation (Fig. S3d), holes and voids in the polymer matrix are notable, where the size of the formed holes in the bulk plastic matches the size of the MNPs that emerged from them (Fig. 3c and d). These features could indicate sites from which MNPs have emerged or serve as pathways for leaching additives such as dyes and processing aids. The observation of particles just below the PE surface suggest these holes may result from additive leaching, further

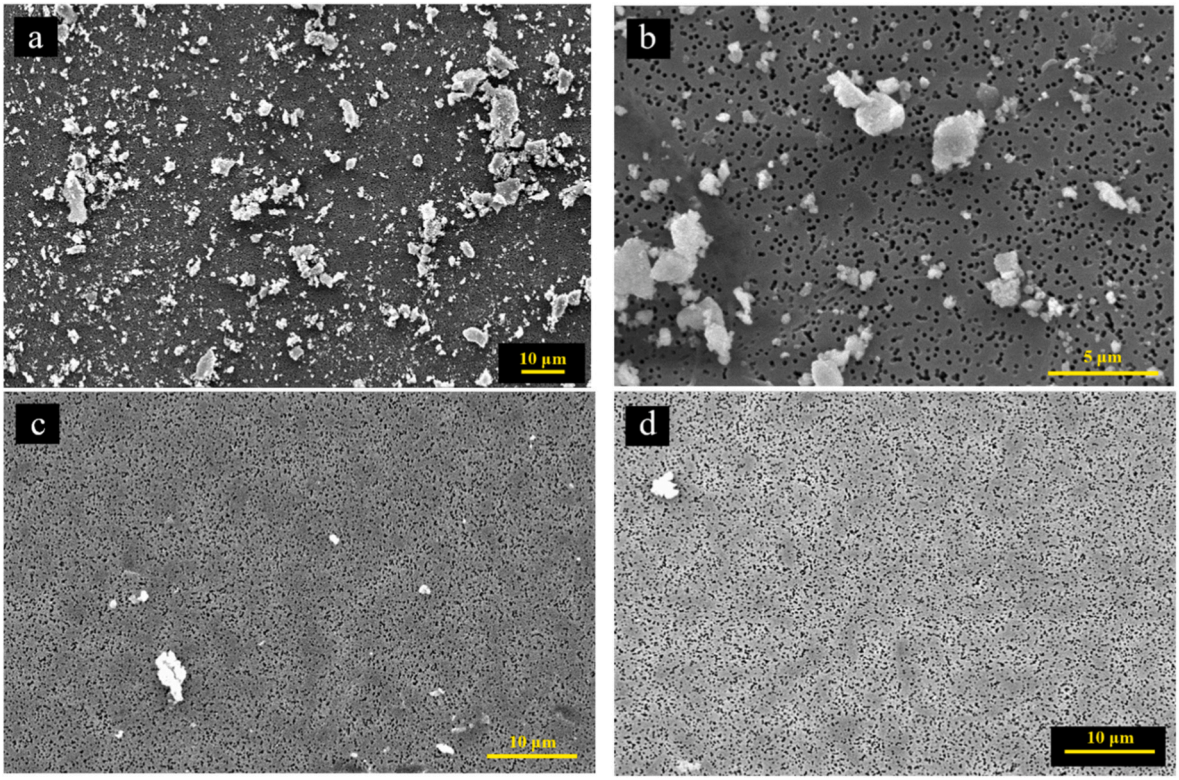

Fig. 3. SEM micrographs of (a) and (b) PET, and (c) and (d) PE MNPs emerged from bulk plastic after 12 weeks of degradation.

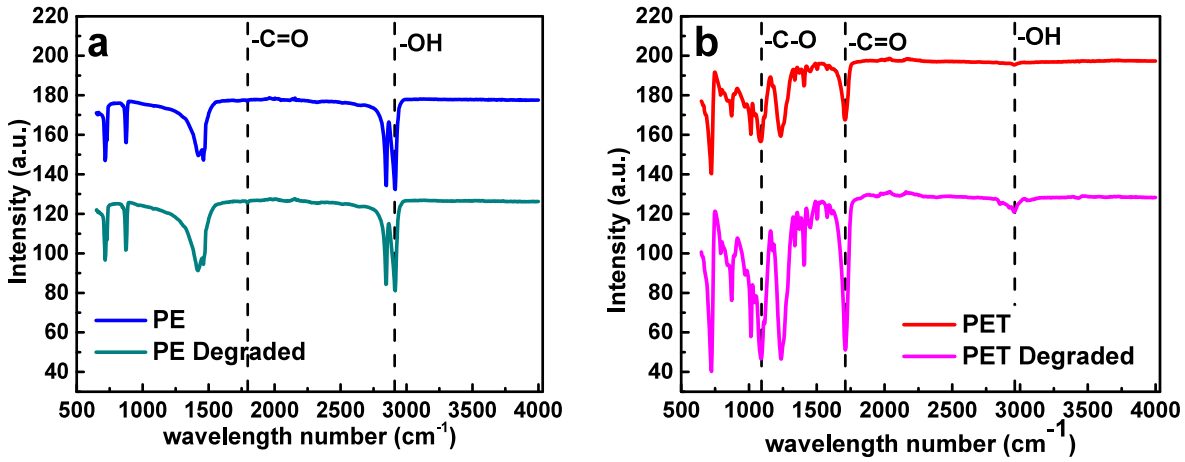

Fig. 4. FTIR spectra of (a) bulk PE (shopping bags) and (b) bulk PET (water bottles) before and after degradation.

substantiating the impact of polymer degradation and bond breakage. Our observation also aligns with other reports on the formation of cracks and holes in PE films after photooxidation (Da Costa et al., 2018).

To further differentiate the effects of mechanical abrasion and photo-oxidation, PE degradation experiments were conducted in the presence of sand under both UV-exposed and dark (no UV and visible lights) conditions. As shown in Fig. S4, the PE surface degraded in presence of sand and UV exhibited pronounced cracking, fissures, and surface roughening, whereas the sample degraded with sand but without UV exposure showed only minor mechanical wear. These results confirm that the presence of UV light accelerates oxidative chain scission and embrittlement, leading to fragmentation, while mechanical abrasion alone contributes primarily to surface wear and particle detachment. The inclusion of sand serves to intensify surface stress and simulate natural sediment interaction, further supporting that photooxidation is the dominant mechanism driving polymer degradation under the simulated conditions.

3.2. Surface chemistry of the polymers

We examined the surface chemistry of the bulk polymers before and after degradation by FTIR. FTIR spectra of samples before and after degradation, as shown in Fig. 4, confirm that photooxidation is the main degradation mechanism, resulting in noticeable alterations in surface chemistry through the introduction of oxygenated functional groups. FTIR spectra of pre- and post-degradation PE samples show the emergence of carbonyl groups at 1745 cm^{-1} and hydroxyl groups at 2700–3000 cm^{-1}, indicating chain scission processes within the polymer matrix (S. Gomes et al., 2024; Tian et al., 2023). Despite a minor peak around 1745 cm^{-1}, the CI (Table 1) does not show a major difference, indicating minimal degradation in PE samples. This is consistent with the lower number of particles emerging from PE, as seen in DLS and SEM results.

In contrast, Fig. 4b shows pre- and post-degradation FTIR spectra of PET samples with clear emergence of carboxyl and carbonyl groups at approximately 1100 cm^{-1} and 1745 cm^{-1}, respectively. The intensification of peaks in the 2700–3000 cm^{-1} range indicates an increased concentration of hydroxyl groups within the polymer. These spectral features confirm polymer degradation through photooxidation, with these oxygenated functional groups resulting from polymer chain scission and molecular transformations. The emergence of oxygenated functional groups is widely reported in the literature, demonstrating consistent trends in forming oxidized functional groups and chemical degradation in both PE and PET under various environmental conditions (Arhant et al., 2019; Da Costa et al., 2018; Miranda et al., 2021; Weinstein et al., 2016).

CI is a useful metric for quantifying the extent of plastic photooxidation. As plastics photo-degrade, oxygen-containing functional groups, such as carbonyls (C=O), are introduced to their backbones. An elevated CI signifies a greater impact by photooxidation, which is correlated with the breakdown of polymer chains during degradation. This process can result in the formation of smaller polymer fragments, such as MNPs (Almond et al., 2020). The variation in the CI across different polymers indicates differences in the degree and type of chemical changes occurring during photo-degradation[21]. As shown in Table 1, the CI for PET increased by 36 %, reflecting the major formation of carbonyl groups. UV exposure causes PET to oxidize, creating carbonyl groups as the polymer chains undergo oxidative degradation, resulting in smaller fragments with carbonyl groups and a higher CI. Conversely, PE showed no change in CI, indicating minimal photooxidation compared to PET, which is consistent with our other experimental observations.

Ainali et al. (2021) thermoformed sheets from PE pellets purchased from petrochemical companies using a hot press technique. These sheets were subjected to 280 nm UV light at an intensity of 260 W/m^2 for 60 days in air while measuring the CI. The results indicated that PE had a CI of approximately 0.002 during the first two weeks, which then increased by 1000 % in the following weeks, marking it as the lowest among the polymers tested, likely due to the UV stabilizers commonly found in agricultural films. This contrasts with our findings, suggesting that variations in degradation conditions and the use of consumer plastics

Table 1
Surface elemental composition, functional groups, and CI of bulk PE and PET before and after degradation.

	PE		PET	
	Pre-degradation	Post-degradation	Pre-degradation	Post-degradation
C/O Ratio	23.9	12.6	5.4	2.9
C–C (at%)	100	95.3	77.1	58.2
C–O (at%)	0	2.2	8.2	17
C=O (at%)	0	2.6	9	12.9
CI	0.002	0.002	0.85	1.16

compared to polymer pellets may account for the differences observed. Additionally, to be closer to actual environmental conditions, we degraded our polymers in water, which in itself is a major UV absorber.

In another study (Luyt et al., 2021), the CI of PE samples with and without UV absorbers was assessed after exposure to UV radiation for up to 85 days using a UV lamp. The samples underwent alternating cycles of UV exposure at an intensity of 0.76 W/m^2 with a wavelength of 340 nm. The CI values for the PE samples without additives rose from zero to 0.85 following UV exposure. In contrast, stabilized samples containing UV absorbers and photo stabilizers exhibited no carbonyl group formation, aligning with our study's results. Additionally, Ding et al. (2022) focused on the photodegradation of PET acquired from a local market in Yangling, China. PET was exposed to UV radiation for up to 7 days, increasing the CI from 0.0151 ± 0.004 at day zero to 0.2052 ± 0.035 at day seven. This increment is consistent with our findings, although the testing conditions differed, as they utilized a 500 W mercury lamp with an intensity of 1000 W/m^2 for photodegradation in air, as opposed to our work which was performed in water. Again, the presence of additives in our PET samples is the reason for the smaller CI in our work.

We used XPS to comprehensively study the surface chemistry of PE and PET samples before and after degradation. Fig. S5 presents XPS survey scans and deconvoluted C_{1s} high-resolution spectra for PET, showing the impact of degradation on surface chemical bonds. Table 1 compares the surface chemistry of PE and PET, pre- and post-degradation.

PE, a thermoplastic polyolefin, primarily consists of ethylene units bonded to carbon via single bonds. Theoretically, it comprises only carbon and hydrogen; however, additives introduce other elements (Ronca, 2017). Table 1 shows a decrease in surface carbon and an increase in oxygen and nitrogen post-degradation, indicating C–C bond cleavage and the formation of C=O or C–O bonds. The decrease in the C/O ratio from 23.9 to 12.55 reflects significant changes in surface chemistry, in line with the presence of carboxyl and hydroxyl groups in FTIR spectra. Deconvolution of the high resolution C_{1s} spectrum confirms the appearance of C–O and C=O bonds after degradation.

PET, composed of terephthalic acid and ethylene glycol units linked by ester bonds, is theoretically comprised of carbon, hydrogen, and oxygen in its structure (Nisticò, 2020). However, additives can alter the elemental composition. XPS results before and after degradation reveal the presence of additives. Like PE, PET shows a decrease in surface carbon and an increase in oxygen post-degradation. Fig. S5 and Table 1 indicate a decrease in the C/O ratio from 4.53 to 2.9, highlighting a significant increase in oxygenated functional groups. Deconvolution of the high resolution C_{1s} spectrum shows a reduction in C–C bonds and an increase in C–O and C=O bonds, which aligns with the FTIR results. Both PE and PET show significant chemical changes upon degradation, as indicated by the decrease in C/O ratios and the emergence of new functional groups such as carbonyl and hydroxyl groups. The extent of these changes in our study is similar to those reported in the literature (Ibrahim, 2024; Kang et al., 2024).

3.3. Measuring the concentration of the MNPs

To analyze the geometrical specification of the MNP, they were manually annotated using the FastSAM option of the V7 labs platform. Typical SEM micrographs and their annotations are presented in Fig. S6, and the summary of the data extracted from image analysis is presented in Table S2. Based on the data in this table, 614 PE particles and 3924 PET particles were analyzed to determine key metrics such as the number of particles, particle size distribution, and surface area. Our calculations showed that the number of counted PE and PET MNPs equals 4.17 and 27.8 million particles per litre, respectively, equivalent to an average concentration of 0.07 ppm PE and 0.18 ppm PET MNPs that emerged from bulk plastics during 12 weeks.

The total number of emerged MNPs was estimated based on the proportional area method described in our previous work (Rezvani et al., 2025). Briefly, a protocol was developed for recording SEM micrographs from fixed locations on the membrane to ensure of the uniformity of the data. In this protocol, SEM micrographs were collected diagonally across the membrane to capture representative areas, assuming a uniform particle distribution. The total number of MNPs in the filtered sample was calculated using equation (1):

$$N_T = N_{IA} \times \frac{A_T}{A_{SEM}} \quad \text{Equation 1}$$

where N_T is the total number of MNPs in the filtered volume, N_{IA} is the number obtained by image analysis, A_T is the total membrane area (18.1 cm^2), and A_{SEM} is the probed area in each micrograph (10^{-6} – 10^{-2} cm^2 depending on magnification). The approach was validated in our earlier study using PS microbeads of known sizes and concentrations (Rezvani et al., 2025), yielding an error below 10 %. Using the measured d_i values, the mass-based concentration was calculated by summing per-particle volumes and multiplying by polymer density, then normalizing by the filtered volume V:

$$C_{\text{mass}} = \left(\frac{\rho}{V} \sum_{i=1}^{N_T} \left(\frac{\pi}{6} d_i^3 \right) \right) \times \frac{A_T}{A_{SEM}} \quad \text{Equation 2}$$

Here ρ is the polymer density (we used $\rho_{PE} = 0.94$ g cm^{-3} and $\rho_{PET} = 1.38$ g cm^{-3}).

Our findings reveal significant differences between PE and PET particles. PET releases a considerably larger number of particles than PE (Fig. 5 and Table S2), suggesting that PET may fragment into smaller pieces more readily. Specifically, PET showed a higher proportion of nanoplastics (particles smaller than 1 μm) at 58 %, compared to 25 % for PE. This suggests that PET is more susceptible to fragmentation into smaller particles, likely due to its distinct degradation mechanism and intrinsic material properties, as reflected by its higher CI compared to PE. CI represents oxidative chain scission and the formation of oxygen-containing groups that weaken intermolecular bonds. For PET, ester linkages are particularly susceptible to hydrolytic and photooxidative cleavage, producing brittle domains that readily fragment into smaller particles. The higher CI of PET (36 % increase) therefore correlates with the higher proportion of nanoplastics observed. In contrast, PE primarily undergoes surface oxidation without significant chain scission, leading to fewer, larger fragments (Arhant et al., 2019; Ding et al., 2022). The mean diameter of PE particles is larger at 3.18 μm, compared to 2.07 μm for PET particles, further supporting the observation that PE degrades into larger fragments than PET.

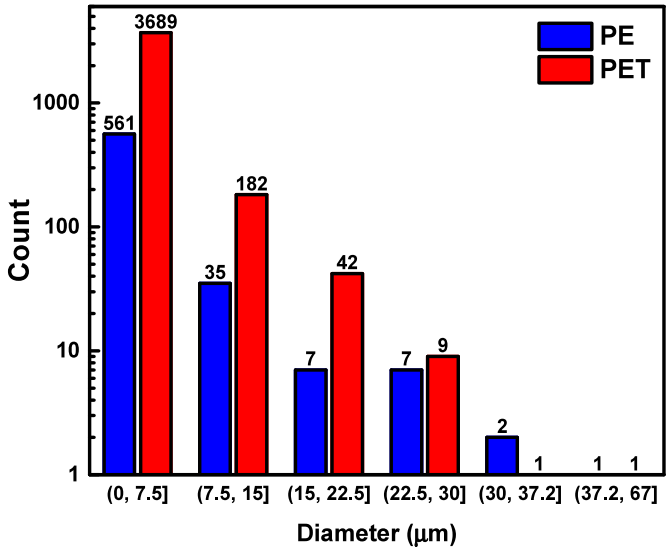

Fig. 5. The size distribution of the MNPs emerged from PE and PET.

Several studies have investigated the release of MPs from PE and PET under various conditions; however, none of them have reported the weathering of bulk polymers in a simulated environment while measuring the concentration of the emerged particles in the micro and nano-size range at the same time (Menzel et al., 2022; Mikac et al., 2024; Miranda et al., 2021; Rahman et al., 2024; Weinstein et al., 2016). This creates a critical gap in the literature, as existing studies primarily focus on larger particles or use methodologies that lack the precision to simulate environmental weathering or to detect submicron particles. Consequently, there is limited data available for direct comparison to our findings. For example, it has been reported that the reusable PET bottles with PP caps released 131–242 MP/L (≥10 μm) after repeated openings, with 80 % of particles measuring 10–50 μm (Winkler et al., 2019).

Several studies have reported the MNP concentration of 0.001–0.1 ppm as environmentally relevant (Abidli et al., 2021; Mak et al., 2019). In one study, researchers assessed the toxicity of PE MNPs (40–50 μm) within this concentration range on Mediterranean mussels (*Mytilus galloprovincialis*) filtration rates and oxidative stress biomarkers (Abidli et al., 2021). Interestingly, the concentrations calculated in our study (0.07 ppm for PE MNPs and 0.18 ppm for PET MNPs) align well with those often cited as environmentally relevant (Abidli et al., 2021). This correspondence highlights the significance of our findings in replicating real-world pollution scenarios. Our approach bridges critical gaps in understanding MNP pollution by extending the analysis into the submicron range. It provides data directly applicable to assessing environmental risks associated with PE and PET polymers.

Calculation of surface area based on image analysis showed that PE particles have a larger mean surface area of 8.31 μm^2 in contrast to 3.69 μm^2 for PET. Larger surface areas can enhance the potential for chemical interactions and adsorption of pollutants, making PE particles significant vectors for transporting harmful contaminants in aquatic environments. The Mann-Whitney *U* test, a non-parametric statistical method, was used to compare the distributions of MNP size and morphology between PE and PET samples, as it does not require normality and is robust for non-parametric data. The tests revealed substantial differences between PE and PET in diameter ($U = 1{,}652{,}250.5$, $p = 9.88 \times 10^{-50}$), area ($U = 1{,}645{,}064.0$, $p = 3.33 \times 10^{-48}$), form factor ($U = 1{,}333{,}882.0$, $p = 1.87 \times 10^{-5}$), and convexity ($U = 951{,}757.5$, $p = 5.36 \times 10^{-17}$), while aspect ratio ($U = 1{,}214{,}023.5$, $p = 0.7564$) and roundness ($U = 1{,}219{,}418.0$, $p = 0.6251$) showed no significant differences. The box plots in Fig. 6 compare the physical characteristics of PE and PET MNPs across six geometrical factors, namely, diameter, area, aspect ratio, form factor, roundness, and convexity. These differences suggest that PE particles might interact differently with the environment, affecting their distribution and impact within ecosystems. PE particles tend to have larger diameters and areas, suggesting they are either initially larger or aggregate more than PET particles. Differences in form factor and convexity imply that PE particles are more irregular in shape, affecting their transport and fate in the environment. Aspect ratio and roundness were similar between PE and PET particles. Understanding the physical characteristics of MNPs is crucial for assessing their environmental impact. The significant differences in size and shape between PE and PET particles can affect their distribution, transport, and interactions within marine and terrestrial ecosystems. Larger and more irregularly shaped PE particles might have a higher tendency to impact marine organisms or settle in different environmental niches compared to PET particles. These interactions can affect the health and survival of aquatic species. Physical characteristics can also influence MNP transport and deposition patterns in various environmental compartments, such as water bodies, sediments, and soil. Understanding these differences helps assess the environmental impact and risks associated with different types of MNPs, guiding policies and mitigation strategies for plastic pollution.

When exposed to UV irradiation, heat, and mechanical stress, PE primarily degrades through oxidation, resulting in a slower breakdown process and larger fragments (Andrady et al., 2022). On the other hand, PET degrades through hydrolysis, photodegradation, and mechanical wear, making it more susceptible to breaking down into smaller particles due to its ester bonds, which are more prone to hydrolytic cleavage (Sutkar et al., 2023).

From an environmental perspective, the higher proportion of PET nanoplastics poses a greater risk due to their ability to penetrate biological membranes, enter cells, and bioaccumulate in the food chain. These nanoplastics present significant ecological hazard as they can enter and accumulate in biological systems. In contrast, marine

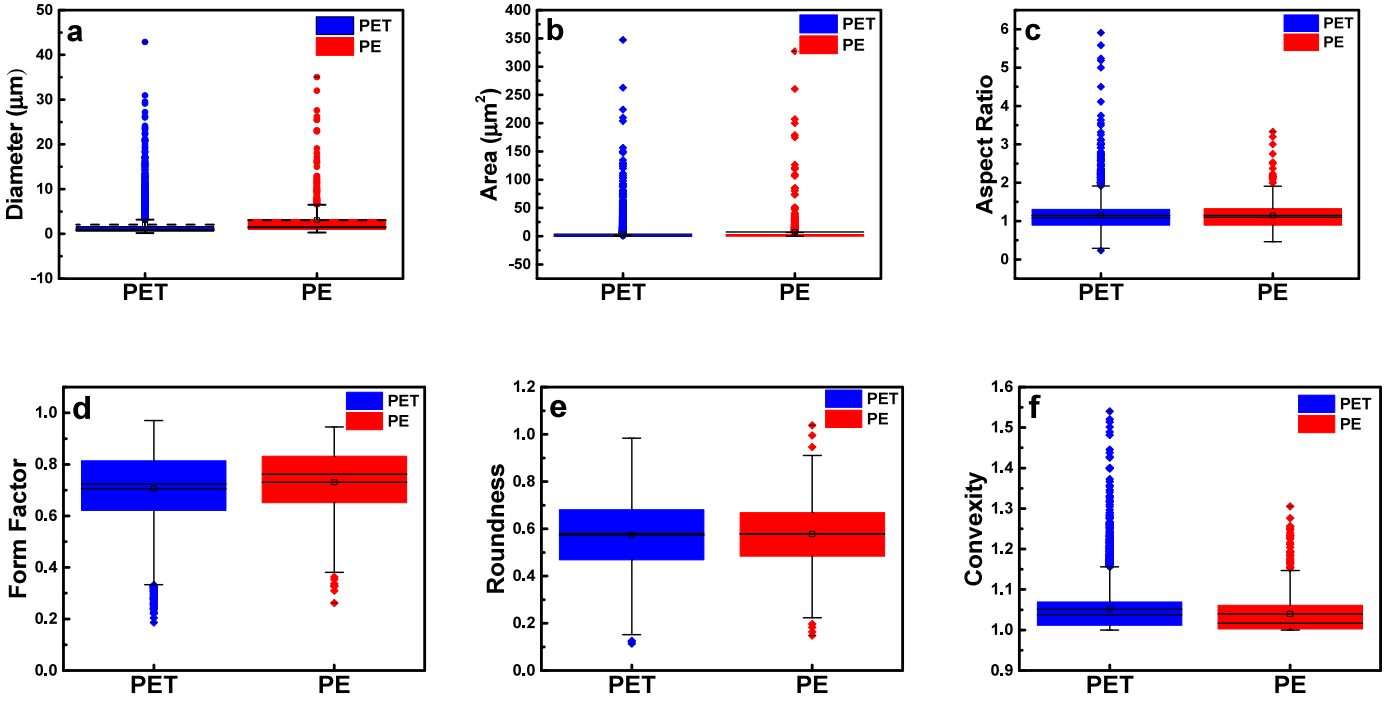

Fig. 6. Morphological characteristics of PE and PET MNPs, including (a) diameter, (b) area, (c) aspect ratio, (d) form factor, (e) roundness, and (f) convexity.

organisms are more likely to ingest PE MPs, potentially causing physical blockages and leaching hazardous chemicals. The larger surface area of PE particles also facilitate the adsorption of pollutants, which can then be transported through aquatic environments. Understanding these differences is crucial for developing targeted strategies to mitigate the environmental impact of plastic pollution.

4. Conclusions

Our comparative PE and PET MNPs analysis highlights significant differences in their degradation behaviours and environmental implications. PET tends to fragment into a larger number of smaller particles, including a substantial proportion of nanoplastics, posing ecological risks due to their potential for bioaccumulation and cellular penetration. While degrading into larger fragments, PE has a larger surface area that enhances its capacity to adsorb pollutants, acting as vectors for transporting harmful substances in aquatic environments. The concentration of MNPs was significantly higher for PET at 27.8 million particles/L (0.18 ppm) compared to 4.17 million particles/L (0.07 ppm) for PE. Characterization using DLS, SEM, XPS, and FTIR provided comprehensive insights into the degradation processes. Using AI enhanced FastSAM for automatic particle annotation significantly improved the efficiency and scalability of MNP analysis, facilitating large-scale environmental monitoring and research. Understanding the distinct degradation mechanisms and ecological behaviours of PE and PET is crucial for developing effective interventions to combat plastic pollution and protect marine ecosystems. Our findings highlight the need for targeted strategies to mitigate the environmental impacts of PE and PET pollution, enhancing our ability to address the challenges posed by plastic waste in aquatic environments.

CRediT authorship contribution statement

Hadi Rezvani: Writing – original draft, Visualization, Validation, Methodology, Investigation, Formal analysis, Data curation, Conceptualization. **Mihir Kapadia:** Validation, Investigation, Data curation. **Julia Costantino:** Validation, Investigation, Data curation. **Navid Zarrabi:** Methodology, Data curation. **Sajad Saeedi:** Writing – review & editing, Supervision, Methodology, Funding acquisition, Conceptualization. **Nariman Yousefi:** Writing – review & editing, Supervision, Methodology, Funding acquisition, Conceptualization.

Declaration of competing interest

The authors declare that they have no known competing financial interests or personal relationships that could have appeared to influence the work reported in this paper.

Acknowledgement

The authors gratefully acknowledge the support of various facilities and individuals who contributed to this work. We thank the Toronto Metropolitan Analytical Centre (TMAC) for providing access to FTIR and the Ontario Centre for the Characterization of Advanced Materials (OCCAM) for assisting with XPS analysis. We thank the TMU SEM Laboratory and Dr. Qing Li for their expertise and guidance in SEM imaging. We also thank Dr. Antimo Graziano for his valuable insight and support throughout this study. The authors acknowledge the financial support from the Research Graduate Scholarship (RGS) and Toronto Metropolitan Graduate Scholarship (TMGS) awards.

This work was supported by the Natural Sciences and Engineering Research Council of Canada (NSERC) Discovery Grants program (grant no. RGPIN-2020-05436), Canada Foundation for Innovation's John R. Evans Leaders Fund (grant no. 39659), Environment and Climate Change Canada's (ECCC) Increasing Knowledge on Plastic Pollution Initiative (contract no. GCXE21S057), and Social Sciences and Humanities Research Council of Canada's (SSHRC) New Frontiers in Research Fund-Exploration program (grant no. NFRFE-2022-00746).

Appendix A. Supplementary data

Supplementary data to this article can be found online at https://doi.org/10.1016/j.envpol.2025.127453.

Data availability

Data will be made available on request.

References

Abidli, S., Pinheiro, M., Lahbib, Y., Neuparth, T., Santos, M.M., Trigui El Menif, N., 2021. Effects of environmentally relevant levels of polyethylene microplastic on Mytilus galloprovincialis (Mollusca: bivalvia): filtration rate and oxidative stress. Environ. Sci. Pollut. Res. Int. 28, 26643–26652. https://doi.org/10.1007/S11356-021-12506-8.

Ainali, N.M., Bikiaris, D.N., Lambropoulou, D.A., 2021. Aging effects on low- and high-density polyethylene, polypropylene and polystyrene under UV irradiation: an insight into decomposition mechanism by Py-GC/MS for microplastic analysis. J. Anal. Appl. Pyrolysis 158, 105207. https://doi.org/10.1016/J.JAAP.2021.105207.

Almond, J., Sugumaar, P., Wenzel, M.N., Hill, G., Wallis, C., 2020. Determination of the carbonyl index of polyethylene and polypropylene using specified area under band methodology with ATR-FTIR spectroscopy. E-Polymers 20, 369–381. https://doi.org/10.1515/EPOLY-2020-0041/MACHINEREADABLECITATION/RIS.

Andrady, A.L., Barnes, P.W., Bornman, J.F., Gouin, T., Madronich, S., White, C.C., Zepp, R.G., Jansen, M.A.K., 2022. Oxidation and fragmentation of plastics in a changing environment; from UV-radiation to biological degradation. Sci. Total Environ. 851, 158022. https://doi.org/10.1016/j.scitotenv.2022.158022.

Archit, A., Freckmann, L., Nair, S., Khalid, N., Hilt, P., Rajashekar, V., Freitag, M., Teuber, C., Buckley, G., von Haaren, S., Gupta, S., Dengel, A., Ahmed, S., Pape, C., 2025. Segment anything for microscopy. Nat. Methods 22, 579–591. https://doi.org/10.1038/S41592-024-02580-4. SUBJMETA.

Arhant, M., Le Gall, M., Le Gac, P.-Y., Davies, P., 2019. Impact of hydrolytic degradation on mechanical properties of PET - towards an understanding of microplastics formation. Polym. Degrad. Stabil. 161, 175–182. https://doi.org/10.1016/j.polymdegradstab.2019.01.021.

Brewer, A., Dror, I., Berkowitz, B., 2021. The mobility of plastic nanoparticles in aqueous and soil environments: a critical review. ACS Environ. Sci. Technol. Water 1, 48–57. https://doi.org/10.1021/ACSESTWATER.0C00130/ASSET/IMAGES/LARGE/EW0C00130_0003.JPEG.

Cai, Y., Yang, T., Mitrano, D.M., Heuberger, M., Hufenus, R., Nowack, B., 2020. Systematic study of microplastic fiber release from 12 different polyester textiles during washing. Environ. Sci. Technol. 54, 4855. https://doi.org/10.1021/ACS.EST.9B07395/ASSET/IMAGES/MEDIUM/ES9B07395_M001.GIF.

Chen, Q., Yang, Y., Qi, H., Su, L., Zuo, C., Shen, X., Chu, W., Li, F., Shi, H., 2024. Rapid mass conversion for environmental microplastics of diverse shapes. Environ. Sci. Technol. 58, 10776–10785. https://doi.org/10.1021/acs.est.4c01031.

Da Costa, J.P., Nunes, A.R., Santos, P.S.M., Girão, A.V., Duarte, A.C., Rocha-Santos, T., 2018. Degradation of polyethylene microplastics in seawater: insights into the environmental degradation of polymers. J Environ Sci Health A Tox Hazard Subst Environ Eng 53, 866–875. https://doi.org/10.1080/10934529.2018.1455381.

Dimassi, S.N., Hahladakis, J.N., Daly Yahia, M.N., Ahmad, M.I., Sayadi, S., Al-Ghouti, M. A., 2023. Insights into the degradation mechanism of PET and PP under marine conditions using FTIR. J. Hazard Mater. 447, 130796. https://doi.org/10.1016/j.jhazmat.2023.130796.

Ding, L., Yu, X., Guo, X., Zhang, Y., Ouyang, Z., Liu, P., Zhang, C., Wang, T., Jia, H., Zhu, L., 2022. The photodegradation processes and mechanisms of polyvinyl chloride and polyethylene terephthalate microplastic in aquatic environments: important role of clay minerals. Water Res. 208, 117879. https://doi.org/10.1016/J.WATRES.2021.117879.

Dube, E., Okuthe, G.E., 2023. Plastics and Micro/Nano-Plastics (MNPs) in the environment: occurrence, impact, and toxicity. Int. J. Environ. Res. Publ. Health 20, 6667. https://doi.org/10.3390/IJERPH20176667.

Gao, Y., Gao, W., Liu, Y., Zou, D., Li, Y., Lin, Y., Zhao, J., 2024. A comprehensive review of microplastic aging: laboratory simulations, physicochemical properties, adsorption mechanisms, and environmental impacts. Sci. Total Environ. 957, 177427. https://doi.org/10.1016/J.SCITOTENV.2024.177427.

Giese, A., Kerpen, J., Weber, F., Prediger, J., 2021. A preliminary Study of microplastic abrasion from the screw cap System of reusable plastic bottles by Raman Microspectroscopy. ACS ES&T Water 1, 1363–1368. https://doi.org/10.1021/acsestwater.0c00238.

Gomes, S., R, Fernandes, A.N., Waldman, W.R., 2024. How to measure polymer degradation? An analysis of authors' choices when calculating the carbonyl index. Environ. Sci. Technol. 58, 7609–7616. https://doi.org/10.1021/acs.est.3c10855.

Hernandez, L.M., Xu, E.G., Larsson, H.C.E., Tahara, R., Maisuria, V.B., Tufenkji, N., 2019. Plastic teabags release billions of microparticles and nanoparticles into tea. Environ. Sci. Technol. 53, 12300–12310. https://doi.org/10.1021/ACS.EST.9B02540/ASSET/IMAGES/LARGE/ES9B02540_0003.JPEG.

Ibor, O.R., Mpama, N.O.L., Okoli, C.P., Ogarekpe, D.M., Edet, U.O., Ajang, R.O., Onyezobi, C.E., Anyanti, J., Idogho, O., Aizobu, D., Arukwe, A., 2023. Occurrence, identification and characterization of plastic pollution from an open solid waste dumpsite in Calabar, Southern Nigeria. Environ. Adv. 11, 100338. https://doi.org/10.1016/J.ENVADV.2022.100338.

Ibrahim, A.M., 2024. Plastics: photodegradations and mechanisms. Microplastics and Pollutants, pp. 25–49. https://doi.org/10.1007/978-3-031-54565-8_2.

Isobe, A., Iwasaki, S., 2022. The fate of missing ocean plastics: are they just a marine environmental problem? Sci. Total Environ. 825, 153935. https://doi.org/10.1016/J.SCITOTENV.2022.153935.

Julienne, F., Delorme, N., Lagarde, F., 2019. From macroplastics to microplastics: role of water in the fragmentation of polyethylene. Chemosphere 236, 124409. https://doi.org/10.1016/j.chemosphere.2019.124409.

Kang, A., Luo, Y., Luo, Q., Li, S., Tang, Y., Yi, F., Zhang, H., Chen, Y., Jia, M., Xiong, W., Yang, Z., Xu, H., 2024. An investigation into the aging mechanism of disposable face masks and the interaction between different influencing factors. J. Hazard Mater. 477, 135308. https://doi.org/10.1016/J.JHAZMAT.2024.135308.

Kelly, M.R., Lant, N.J., Kurr, M., Burgess, J.G., 2019. Importance of water-volume on the release of microplastic fibers from Laundry. Environ. Sci. Technol. 53, 11735–11744. https://doi.org/10.1021/ACS.EST.9B03022/SUPPL_FILE/ES9B03022_SI_001.PDF.

Kibria, M.G., Masuk, N.I., Safayet, R., Nguyen, H.Q., Mourshed, M., 2023. Plastic waste: challenges and opportunities to mitigate pollution and effective management. Int. J. Environ. Res. 17, 20. https://doi.org/10.1007/s41742-023-00507-z.

Kirillov, A., Mintun, E., Ravi, N., Mao, H., Rolland, C., Gustafson, L., Xiao, T., Whitehead, S., Berg, A.C., Lo, W.Y., Dollár, P., Girshick, R., 2023. Segment anything. Proc. IEEE International Conf. Computer Vision 3992–4003. https://doi.org/10.1109/ICCV51070.2023.00371.

Knight, L.J., Parker-Jurd, F.N.F., Al-Sid-Cheikh, M., Thompson, R.C., 2020. Tyre wear particles: an abundant yet widely unreported microplastic? Environ. Sci. Pollut. Control Ser. 27, 18345–18354. https://doi.org/10.1007/s11356-020-08187-4.

Li, R., Espi, Wayman, C., Niemann, H., 2021. The fate of plastic in the ocean environment – a minireview. Environ Sci Process Impacts 23, 198–212. https://doi.org/10.1039/D0EM00446D.

Liu, F., Rasmussen, L.A., Klemmensen, N.D.R., Zhao, G., Nielsen, R., Vianello, A., Rist, S., Vollertsen, J., 2023. Shapes of hyperspectral imaged microplastics. Environ. Sci. Technol. 57, 12431–12441. https://doi.org/10.1021/acs.est.3c03517.

Luyt, A.S., Gasmi, S.A., Malik, S.S., Aljindi, R.M., Ouederni, M., Vouyiouka, S.N., Porfyris, A.D., Pfaendner, R., Papaspyrides, C.D., 2021. Artificial weathering and accelerated heat aging studies on low-density polyethylene (Ldpe) produced via autoclave and tubular process technologies. Express Polym. Lett. 15, 121–136. https://doi.org/10.3144/EXPRESSPOLYMLETT.2021.12.

Maddison, C., Sathish, C.I., Lakshmi, D., Wayne, O., Palanisami, T., 2023. An advanced analytical approach to assess the long-term degradation of microplastics in the marine environment. npj Mater. Degrad. 7, 1–11. https://doi.org/10.1038/s41529-023-00377-y.

Mak, C.W., Ching-Fong Yeung, K., Chan, K.M., 2019. Acute toxic effects of polyethylene microplastic on adult zebrafish. Ecotoxicol. Environ. Saf. 182, 109442. https://doi.org/10.1016/J.ECOENV.2019.109442.

Malli Mohan, G.B., Stricker, M.C., Venkateswaran, K., 2019. Microscopic characterization of biological and inert particles associated with spacecraft assembly cleanroom. Sci. Rep. 9, 1–13. https://doi.org/10.1038/S41598-019-50782-0. TECHMETA.

Mann, H.B., Whitney, D.R., 1947. On a Test of whether one of two random variables is stochastically larger than the other. Ann. Math. Stat. 18, 50–60. https://doi.org/10.1214/AOMS/1177730491.

Mason, S.A., Welch, V.G., Neratko, J., 2018. Synthetic polymer contamination in bottled water. Front. Chem. 6, 407. https://doi.org/10.3389/FCHEM.2018.00407.

Menzel, T., Meides, N., Mauel, A., Mansfeld, U., Kretschmer, W., Kuhn, M., Herzig, E.M., Altstädt, V., Strohriegl, P., Senker, J., Ruckdäschel, H., 2022. Degradation of low-density polyethylene to nanoplastic particles by accelerated weathering. Sci. Total Environ. 826, 154035. https://doi.org/10.1016/J.SCITOTENV.2022.154035.

Mikac, L., Csáki, A., Zentai, B., Rigó, I., Veres, M., Tolić, A., Gotić, M., Ivanda, M., 2024. UV irradiation of polyethylene terephthalate and polypropylene and detection of formed microplastic particles Down to 1 μm. ChemPlusChem 89, e202300497. https://doi.org/10.1002/CPLU.202300497.

Mintenig, S.M., Bäuerlein, P.S., Koelmans, A.A., Dekker, S.C., Van Wezel, A.P., 2018. Closing the gap between small and smaller: towards a framework to analyse nano- and microplastics in aqueous environmental samples. Environ. Sci. Nano 5, 1640–1649. https://doi.org/10.1039/C8EN00186C.

Miranda, M.N., Sampaio, M.J., Tavares, P.B., Silva, A.M.T., Pereira, M.F.R., 2021. Aging assessment of microplastics (LDPE, PET and uPVC) under urban environment stressors. Sci. Total Environ. 796, 148914. https://doi.org/10.1016/j.scitotenv.2021.148914.

Nisticò, R., 2020. Polyethylene terephthalate (PET) in the packaging industry. Polym. Test. 90, 106707. https://doi.org/10.1016/j.polymertesting.2020.106707.

Novakovic, K., Thumbarathy, D., Peeters, M., Geoghegan, M., Go Jefferies, J., Hicks, C., Manika, D., Dai, S., 2023. Zero-waste circular economy of plastic packaging: the bottlenecks and a way forward. Sustain. Mater. Technol. 38, e00735. https://doi.org/10.1016/j.susmat.2023.e00735.

Rahman, E., BinAhmed, S., Keyes, P., Alberg, C., Godfreey-Igwe, S., Haugstad, G., Xiong, B., 2024. Nanoscale abrasive wear of polyethylene: a novel approach to probe nanoplastic release at the single asperity level. Environ. Sci. Technol. https://doi.org/10.1021/ACS.EST.3C09649/SUPPL_FILE/ES3C09649_SI_001.PDF.

Rezvani, H., Zarrabi, N., Mehta, I., Kolios, C., Jaafar, H.A., Kao, C.-H., Saeedi, S., Yousefi, N., 2024. Morphological detection and classification of microplastics and nanoplastics emerged from consumer products by deep learning. arXiv Preprint. https://doi.org/10.48550/arXiv.2409.13688.

Rezvani, H., Kapadia, M., Costantino, J., Yousefi, N., 2025. Environmental photodegradation of commercial food containers: analytical, quantitative, and morphological analysis of emerged microplastics and nanoplastics. https://doi.org/10.2139/SSRN.5146229.

Ronca, S., 2017. Chapter 10 - polyethylene. In: Gilbert, M. (Ed.), Brydson's Plastics Materials, eighth ed. Butterworth-Heinemann, pp. 247–278. https://doi.org/10.1016/B978-0-323-35824-8.00010-4.

Schymanski, D., Goldbeck, C., Humpf, H.U., Fürst, P., 2018. Analysis of microplastics in water by micro-raman spectroscopy: release of plastic particles from different packaging into mineral water. Water Res. 129, 154–162. https://doi.org/10.1016/J.WATRES.2017.11.011.

Sutkar, P.R., Gadewar, R.D., Dhulap, V.P., 2023. Recent trends in degradation of microplastics in the environment: a state-of-the-art review. J. Hazard. Mater. Adv. 11. https://doi.org/10.1016/J.HAZADV.2023.100343.

Tian, R., Li, K., Lin, Y., Lu, C., Duan, X., 2023. Characterization techniques of polymer aging: from beginning to end. Chem. Rev. 123, 3007–3088. https://doi.org/10.1021/acs.chemrev.2c00750.

V7 Darwin, 2023. AI data Labeling & ML training data platform [WWW Document]. https://www.v7labs.com/, 9.4.25.

Weinstein, J.E., Crocker, B.K., Gray, A.D., 2016. From macroplastic to microplastic: degradation of high-density polyethylene, polypropylene, and polystyrene in a salt marsh habitat. Environ. Toxicol. Chem. 35, 1632–1640. https://doi.org/10.1002/etc.3432.

Winkler, A., Santo, N., Ortenzi, M.A., Bolzoni, E., Bacchetta, R., Tremolada, P., 2019. Does mechanical stress cause microplastic release from plastic water bottles? Water Res. 166, 115082. https://doi.org/10.1016/j.watres.2019.115082.

Xu, Y., Ou, Q., van der Hoek, J.P., Liu, G., Lompe, K.M., 2024. Photo-oxidation of Micro- and nanoplastics: physical, chemical, and biological effects in environments. Environ. Sci. Technol. 58, 991–1009. https://doi.org/10.1021/acs.est.3c07035.

Yong, C.Q.Y., Valiyaveettil, S., Tang, B.L., 2020. Toxicity of microplastics and nanoplastics in Mammalian systems. Int. J. Environ. Res. Public Health 2020 17. https://doi.org/10.3390/IJERPH17051509. Page 1509 17, 1509.

Zhang, R., Chen, X., Tang, X., Chen, Q., Guo, S., Liu, C., Guo, Z., Zhou, Y., Zhou, X., 2025. Research on intelligent identification of microscopic substances in shale scanning electron microscope images based on deep learning theory. Sci. Rep. 15, 1–11. https://doi.org/10.1038/S41598-025-91225-3. SUBJMETA.